The Astronomical Journal, 166:84 (11pp), 2023 September https://doi.org/10.3847/1538-3881/ace347

A VERITAS/Breakthrough Listen Search for Optical Technosignatures

A. Acharyya[1], C. B. Adams[2], A. Archer[3], P. Bangale[4], P. Batista[5], W. Benbow[6], A. Brill[7], M. Capasso[8], M. Errando[9], A. Falcone[10], Q. Feng[6], J. P. Finley[11], G. M. Foote[4], L. Fortson[12], A. Furniss[13], S. Griffin[14], W. Hanlon[6], D. Hanna[15], O. Hervet[16], C. E. Hinrichs[6,17], J. Hoang[16], J. Holder[4], T. B. Humensky[18,19], W. Jin[1], P. Kaaret[20], M. Kertzman[3], M. Kherlakian[5], D. Kieda[21], T. K. Kleiner[5], N. Korzoun[4], S. Kumar[22], M. J. Lang[23], M. Lundy[15], G. Maier[5], C. E. McGrath[24], M. J. Millard[20], H. R. Miller[16], J. Millis[25], C. L. Mooney[4], P. Moriarty[23], R. Mukherjee[8], S. O'Brien[15,26], R. A. Ong[26], M. Pohl[5,27], E. Pueschel[5], J. Quinn[23], K. Ragan[15], P. T. Reynolds[28], D. Ribeiro[12], E. Roache[6], J. L. Ryan[26], I. Sadeh[5], L. Saha[6], M. Santander[1], G. H. Sembroski[11], R. Shang[8], D. Tak[5], A. K. Talluri[12], J. V. Tucci[29], N. Vazquez[16], D. A. Williams[16], S. L. Wong[15], J. Woo[30]
VERITAS Collaboration,
D. DeBoer[31], H. Isaacson[31,32], I. de Pater[33], D. C. Price[34,35], and A. Siemion[31,36,37,38]
[1] Department of Physics and Astronomy, University of Alabama, Tuscaloosa, AL 35487, USA
[2] Physics Department, Columbia University, New York, NY 10027, USA
[3] Department of Physics and Astronomy, DePauw University, Greencastle, IN 46135-0037, USA
[4] Department of Physics and Astronomy and the Bartol Research Institute, University of Delaware, Newark, DE 19716, USA; gregoryf@udel.edu
[5] DESY, Platanenallee 6, D-15738 Zeuthen, Germany
[6] Center for Astrophysics | Harvard & Smithsonian, Cambridge, MA 02138, USA
[7] N.A.S.A./Goddard Space-Flight Center, Code 661, Greenbelt, MD 20771, USA
[8] Department of Physics and Astronomy, Barnard College, Columbia University, NY 10027, USA
[9] Department of Physics, Washington University, St. Louis, MO 63130, USA
[10] Department of Astronomy and Astrophysics, 525 Davey Lab, Pennsylvania State University, University Park, PA 16802, USA
[11] Department of Physics and Astronomy, Purdue University, West Lafayette, IN 47907, USA
[12] School of Physics and Astronomy, University of Minnesota, Minneapolis, MN 55455, USA
[13] Department of Physics, California State University—East Bay, Hayward, CA 94542, USA
[14] WIPAC and Department of Physics, University of Wisconsin-Madison, Madison, WI 53703, USA
[15] Physics Department, McGill University, Montreal, QC H3A 2T8, Canada
[16] Santa Cruz Institute for Particle Physics and Department of Physics, University of California, Santa Cruz, CA 95064, USA
[17] Department of Physics and Astronomy, Dartmouth College, 6127 Wilder Laboratory, Hanover, NH 03755 USA
[18] Department of Physics, University of Maryland, College Park, MD, USA
[19] NASA GSFC, Greenbelt, MD 20771, USA
[20] Department of Physics and Astronomy, University of Iowa, Van Allen Hall, Iowa City, IA 52242, USA
[21] Department of Physics and Astronomy, University of Utah, Salt Lake City, UT 84112, USA
[22] School of Natural Sciences, University of Galway, University Road, Galway, H91 TK33, Ireland
[23] School of Physics, University College Dublin, Belfield, Dublin 4, Ireland
[24] Department of Physics and Astronomy, Ball State University, Muncie, IN 47306, USA
[25] Arthur B. McDonald Canadian Astroparticle Physics Research Institute, 64 Bader Lane, Queen's University, Kingston, ON K7L 3N6, Canada
[26] Department of Physics and Astronomy, University of California, Los Angeles, CA 90095, USA
[27] Institute of Physics and Astronomy, University of Potsdam, D-14476 Potsdam-Golm, Germany
[28] Department of Physical Sciences, Munster Technological University, Bishopstown, Cork, T12 P928, Ireland
[29] Department of Physics, Indiana University-Purdue University Indianapolis, Indianapolis, IN 46202, USA
[30] Columbia Astrophysics Laboratory, Columbia University, New York, NY 10027, USA
[31] Breakthrough Listen, University of California Berkeley, Berkeley, CA 94720, USA
[32] University of Southern Queensland, Toowoomba, QLD 4350, Australia
[33] Department of Astronomy, University of California Berkeley, Berkeley, CA 94720, USA
[34] International Centre for Radio Astronomy Research, Curtin University, Kent Street, Bentley WA 6102, Australia
[35] Radio Astronomy Laboratory, 501 Campbell Hall, University of California, Berkeley, CA 94720, USA
[36] SETI Institute, Mountain View, CA 94043, USA
[37] Department of Physics and Astronomy, University of Manchester, UK
[38] University of Malta, Institute of Space Sciences and Astronomy, Msida, MSD2080, Malta
Received 2023 May 9; revised 2023 June 26; accepted 2023 June 29; published 2023 August 1

Abstract

The Breakthrough Listen Initiative is conducting a program using multiple telescopes around the world to search for "technosignatures": artificial transmitters of extraterrestrial origin from beyond our solar system. The Very Energetic Radiation Imaging Telescope Array System (VERITAS) Collaboration joined this program in 2018 and provides the capability to search for one particular technosignature: optical pulses of a few nanoseconds in duration detectable over interstellar distances. We report here on the analysis and results of dedicated VERITAS observations of Breakthrough Listen targets conducted in 2019 and 2020 and of archival VERITAS data collected since 2012. Thirty hours of dedicated observations of 136 targets and 249 archival observations of 140 targets were analyzed and did not reveal any signals consistent with a technosignature. The results are used to place limits on

the fraction of stars hosting transmitting civilizations. We also discuss the minimum pulse sensitivity of our observations and present VERITAS observations of CALIOP: a space-based pulsed laser on board the Cloud-Aerosol Lidar and Infrared Pathfinder Satellite Observations. The detection of these pulses with VERITAS, using the analysis techniques developed for our technosignature search, allows a test of our analysis efficiency and serves as an important proof of principle.

Unified Astronomy Thesaurus concepts: Technosignatures (2128); Search for extraterrestrial intelligence (2127); Gamma-ray telescopes (634); Transient detection (1957)

1. Introduction

The search for extraterrestrial intelligence (SETI) can be defined as the "theory and practice of searching for extraterrestrial technology or technosignatures" (Wright et al. 2018b). Technosignatures are extraterrestrial signals whose only explanation is that they were produced artificially. Examples of potential technosignatures include interstellar radio-based communications (Cocconi & Morrison 1959), interstellar laser-based communications (Schwartz & Townes 1961; Tellis & Marcy 2017; Zuckerman et al. 2023), radio and optical leakage from technological civilizations (Sullivan et al. 1978; Schneider et al. 2010), infrared emission from Dyson spheres (Dyson 1960), spectral evidence for industrial pollutants in exoplanet atmospheres (Wright 2018), and physical artifacts deposited within our solar system (Bracewell 1960). Since the founding of the field in the 1950s, there have been numerous searches for these technosignatures using radio, optical, and infrared telescopes, but the fraction of the total parameter space that has been searched remains extremely low (Wright et al. 2018a).

This paper presents the results of a partnership between the Very Energetic Radiation Imaging Telescope Array System (VERITAS) Collaboration and the Breakthrough Listen Initiative in a search for pulsed optical laser-based communications. The Breakthrough Listen Initiative[39] is currently the foremost technosignature search campaign (Worden et al. 2017; Isaacson et al. 2017). It began searching for radio technosignatures in 2016 through a partnership with the Green Bank Telescope and the Parkes Observatory, subsequently adding MEERKAT in 2018. Similarly in the optical band, a partnership with the Automated Planet Finder in 2016 at the Lick Observatory and the Keck Observatory enabled a spectral search for laser-based communication (Tellis & Marcy 2017; Isaacson et al. 2019; Lipman et al. 2019). More recently, Breakthrough has partnered with the exoplanet-hunting Transiting Exoplanet Survey Satellite (TESS) to search for anomalous stellar light curves and to search targets of interest from the TESS catalog with radio telescopes (Traas et al. 2021; Franz et al. 2022). Taken together, these partnerships constitute the most comprehensive search for technosignatures thus far (Gajjar et al. 2019).

Each search for a specific technosignature has benefits and drawbacks, justifying the approach of performing many such searches concurrently. For example, radio-leakage technosignatures emit continuously in every direction, but the inverse-square law and the expected low radio intensity lead to a requirement for radio telescopes that are still in the planning and construction phases, with the full Square Kilometer Array being a notable example (Siemion et al. 2015).

For pulsed optical laser-based communication, the benefit lies in concentrating all of the emitting power into a small angular diameter over nanosecond timescales. These laser pulses could, in principle, be produced with today's technology, and could be easily distinguished from the emitter's host star, without significant dispersion losses. A 3 ns, 3.7 MJ optical laser pulse, collimated at the source using a 10 m reflector and observed from a distance of 1000 lt-yr, would appear approximately 10^4 times as bright as its host star (Horowitz et al. 2001; Howard et al. 2004). Constructing an interstellar communication system based on this technology is not only theoretically possible but is currently feasible. While these pulses could be bright when observed from within the beam's solid angle, they would occur only over very short timescales. The optical receiver therefore requires a large-aperture mirror with fast photon detectors and associated instrumentation. These requirements are the same as those for atmospheric Cherenkov telescopes (ACTs), which are used to measure nanosecond-timescale Cherenkov emission from cosmic-ray-initiated and gamma-ray-initiated particle showers in the Earth's atmosphere. These telescopes can therefore be used to search for optical laser pulse technosignatures (Covault 2001; Eichler & Beskin 2001; Holder et al. 2005; Armada et al. 2005).

Nanosecond pulsed SETI searches in the blue/UV region of the electromagnetic spectrum in particular are well motivated, if the background due to cosmic-ray events can be removed. The study of cosmic rays has been ongoing for more than a century and is closely tied to the development of modern physics. Cosmic rays are an important and ubiquitous constituent of the Galaxy—their energy density is similar to that of starlight, Galactic magnetic fields, or the cosmic microwave background radiation. Any developing technological civilization would almost certainly study cosmic rays and, if located on a planet with a transparent atmosphere, would very likely use the atmospheric Cherenkov effect to do so. The key technology required for this—photomultiplier tubes—has been widely available to our civilization since the late 1930s. Furthermore, Cherenkov telescopes are (by far) the largest *optical* telescopes in the world. The High Energy Stereoscopic System (HESS) II telescope, currently operating, has a remarkable 28 m aperture and the field as a whole has been operating 10 m class telescopes since the late 1960s. We argue, therefore, that nanosecond pulsed emission in the blue/UV (at the peak of the spectrum of Cherenkov light) represents a preferred search region for SETI, similar to the famous "water hole" in the radio band.

Other wavelengths, such as the near-infrared, might also be a natural choice as they experience less extinction due to dust. However, we also argue that any advanced civilization attempting to communicate with an emerging technological civilization would be aware that Cherenkov telescopes are one of the earliest methods capable of easily detecting signals over interstellar distances and that these observations will occur

[39] https://breakthroughinitiatives.org/

naturally as a side project of fundamental physical investigations.

One of the first such searches was conducted using the Solar Tower Atmospheric Cherenkov Effect Experiment (STACEE), which repurposed a New Mexico solar energy research facility for nighttime operations as a wave-front-sampling ACT (Gingrich et al. 2005). STACEE consisted of a field of 64 steerable heliostats, each with a $37\,m^2$ mirror area. Light received at the heliostats was reflected onto two sets of secondary mirrors at the top of a tower before being focused onto a set of 64 photomultiplier tubes (PMTs). This system had a 10–15 photon m^{-2} sensitivity between 400 and 500 nm, peaking at 420 nm. The STACEE Collaboration conducted dedicated observations of 187 targets from the HabCat catalog (Turnbull & Tarter 2003) for 10 minutes each, between 2007 January and May, and did not find any evidence for technosignature signals during their observations (Hanna et al. 2009).

Imaging atmospheric Cherenkov telescopes are also designed to detect atmospheric Cherenkov radiation, but differ from wave-front samplers such as STACEE in that the telescopes are equipped with photomultiplier tube cameras, which allow recording of an image of the Cherenkov light flash. The potential use of such imaging ACTs (IACTs) for SETI for technosignature searches was first discussed in the early 2000s (Tarter 2003), and an analysis methodology and a single test observation using the Whipple 10 m IACT was performed in 2005 (Holder et al. 2005). The importance of the imaging technique is that it provides efficient discrimination between point-like pulsed optical technosignatures and the enormous background of Cherenkov flashes generated by cosmic-ray particle showers in the Earth's atmosphere.

The power of IACTs for optical technosignature searches is dramatically improved when multiple telescopes are combined together in an array. An array of physically separated telescopes provides an additional coincidence requirement for the pulses detected by each telescope, combined with the ability to measure parallax. This approach was first developed using the VERITAS array, in an archival search for pulsed optical technosignatures from KIC 8462852 (Abeysekara et al. 2016). The analysis allowed efficient identification of laser-like events over the background of cosmic-ray images.

The VERITAS Collaboration has since partnered with the Breakthrough Listen Initiative to continue the research started with the study of KIC 8462852. This partnership has led to 30 hr of dedicated observations of Breakthrough Listen targets with VERITAS and an analysis of 110 hr of observations from the VERITAS archive of sky regions containing Breakthrough Listen targets. The analysis and first results of this program are reported here.

2. VERITAS

VERITAS is an IACT array, designed to detect Cherenkov radiation from particle showers in the Earth's atmosphere and to identify those initiated by gamma-ray photons over the background of those due to cosmic rays. A description of the VERITAS telescopes can be found in Holder et al. (2006), and the methods of ground-based gamma-ray astronomy are summarized in e.g., Holder (2021). Here we briefly describe those technical aspects of VERITAS most relevant to the search for optical technosignatures.

VERITAS consists of four IACTs located at the Fred Lawrence Whipple Observatory in southern Arizona (Figure 1). Each telescope has a 12 m diameter tessellated reflector mounted on a steerable alt-azimuth platform. The reflector dish comprises 345 hexagonal mirror segments (Roache et al. 2008) arranged in a Davies–Cotton design (Davies & Cotton 1957), giving a total mirror area of $\sim 110\,m^2$. Alignment of the individual mirror segments is performed and regularly verified using the method described by McCann et al. (2010), resulting in an on-axis optical point-spread function (PSF) of less than $0.^\circ 1$ (68% containment radius). The focal length of the optical system is 12 m, giving a focal ratio of 1.0. The focal plane is instrumented with a close-packed array of 499 Hamamatsu R10560 super-bi-alkali photomultiplier tubes (PMTs), covering an approximately circular $3.^\circ 5$-diameter field of view (FOV) with a pixel spacing of $0.^\circ 15$. CCD cameras installed on the telescope structure monitor the position of the PMT camera with respect to the sky and provide pointing corrections with an absolute positional accuracy of $\sim 50''$. The camera PMT pixels are sensitive over a wide spectral range, with a peak detection efficiency around 400 nm. Dead space between the circular entrance windows of the PMTs is reduced by the addition of truncated Winston cones to the PMT front faces. These cones are shaped such that the entrance is hexagonal and the exit is circular, allowing them to effectively tile the FOV (Nagai et al. 2008).

All PMT signals are digitized using 2 ns sampling, 8-bit flash analog-to-digital converters (FADCs). The FADC readout is initiated by a three-level trigger system, which requires a signal at the individual pixel level, the telescope camera level, and over the full array. The individual pixel trigger condition is determined by a constant fraction discriminator, while the telescope camera trigger requires at least three adjacent PMT pixel triggers within a coincidence time window of ~ 5 ns. The array trigger requires at least two telescope camera triggers within a 50 ns coincidence window, after the application of hardware timing delays to correct for path-length differences between telescopes. Since the optical technosignature images are expected to resemble the telescope optical PSF (which can be smaller than the angular size of a single PMT pixel) the impact of the 3 pixel camera-level trigger requirement is particularly important for technosignature searches. We discuss this issue in more detail in Section 4 of this paper.

The recorded FADC pulses are calibrated, integrated, and used to create a 499 pixel image for all four telescopes in the array. These images (or "events") are recorded at a rate of typically 300 Hz, the vast majority of which are due to Cherenkov emission from cosmic-ray-initiated particle cascades in the atmosphere (Kieda 2013). Subsequent analysis of these images allows identification of the small fraction (typically $<10^{-4}$) that are due to gamma-ray-initiated showers or, as described in the following section, to search for images that resemble a distant optical laser pulse.

3. OSETI Analysis with VERITAS

The analysis applied in this work is similar to that used in the original search for optical technosignatures from KIC 8462852 with VERITAS (Abeysekara et al. 2016). The data are first reduced using the standard VERITAS analysis packages (Maier & Holder 2017; Cogan 2008), which calibrate and parameterize the recorded images using a moment analysis. Cuts on the resulting image parameters (the image *width*, *length*, etc.—

Figure 1. Elevated view of the VERITAS array located at the base of Mount Hopkins near Tucson, AZ. Pictured are the four individual telescopes, which are roughly 100 m apart, the Fred Lawrence Whipple Observatory visitor center, and the VERITAS control building (with the white roof). Image from Abeysekara et al. (2016).

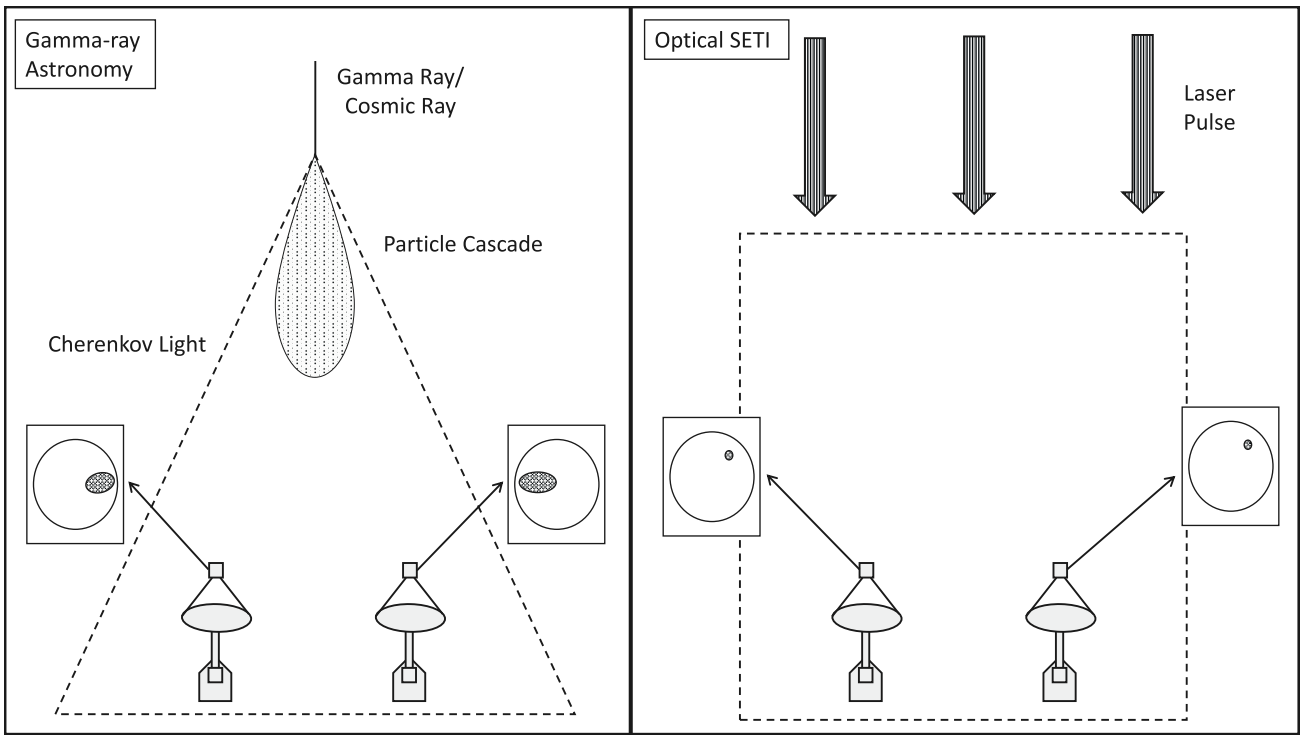

Figure 2. Schematic illustration of the optical SETI (OSETI) technique with IACT arrays such as VERITAS. Particle air showers, initiated by cosmic-ray particles or gamma-ray photons, produce extended images with parallax shifts when viewed from separated telescopes (left). A distant laser pulse produces identical point-like images, located at the same position in the field of view in each telescope (right).

usually referred to as Hillas parameters; Hillas 1985) are then used to filter almost all events due to Cherenkov emission from cosmic-ray air showers from the data. While more sophisticated machine learning approaches are under investigation for this analysis, and are already in use for VERITAS gamma-ray analyses (Krause et al. 2017), simple image parameter cut selections are computationally cheap and robust, and have proven to be extremely effective.

The key characteristics of a potential optical technosignature are: (i) that the emission is point-like (i.e., indistinguishable from the telescope optical PSF); (ii) that it originates from infinity (i.e., shows no parallax shift and has uniform intensity, when viewed from different locations on the ground); and (iii) that it originates from the position of a target star. This is in contrast to the Cherenkov radiation images of particle cascades produced locally in the Earth's atmosphere, which can have a large angular extent (up to a few degrees), are uniformly distributed over the FOV, and display significant parallax and nonuniform intensity when viewed by separated telescopes. Although not used in our work, pulse timing differences may also be used to identify technosignature candidates (Wright et al. 2018c). These features are illustrated schematically in Figure 2.

The choice of image parameter cuts follows logically from these differences. In the analysis of KIC 8462852, the cuts required that at least three of the four telescope images must contain light, the centroid coordinates of the images in every telescope must be separated from each other by less than $0\overset{\circ}{.}15$, and the *length* and *width* of all images must be less than $0\overset{\circ}{.}1125$. After the removal of a few examples of easily

identified meteor and satellite tracks, only 28 of the initial 7036970 events passed these selection cuts. There were no events retained in which the average position of the images was within $0.^{\circ}15$ of the location of the target star for that study, KIC 8462852.

In this work, we are analyzing a much larger data set, testing a catalog of many targets, and have a less homogeneous set of observations. These factors motivate the application of stricter cuts to further improve background rejection. The most important of these is a modification to the *length* and *width* cuts. First, we reduce the cut values to length $< 0.^{\circ}09$ and width $< 0.^{\circ}07$, this matches the optical PSF of the telescopes better than before. Second, we apply these cuts to the telescope with the third-smallest measured *length* or *width* in each event. The motivation behind this is to reduce the impact of PMT afterpulses in the data. Afterpulses are a well-known phenomenon caused mainly by residual positive ions in the PMTs. They appear in the telescope cameras as a single, relatively bright pixel, randomly located in the field of view. This can distort the Hillas parameters of the image in the affected telescope. However, afterpulsing typically affects at most one telescope image in a given event. Applying the *length* and *width* cuts to the image with the third-smallest values of these parameters allows an event with one afterpulse-contaminated image to be retained. The telescope image that exceeds the *length* and *width* cuts is then also removed from consideration for the other selection criteria. An additional modification is to remove any events that include images potentially truncated by the edge of the camera. This is implemented using the *loss* parameter, defined as the fraction of the total light in the image contained in pixels that lie on the edge of the camera (we require loss = 0). As a final check, we visually inspect any remaining candidate events (and their associated ancillary data) to ensure that the telescope cameras were functioning correctly and that each telescope contributed to the event as expected. For example, if a bright pulse was recorded in only three of the four telescopes, this would exclude it as a candidate—except if the missing telescope had an inoperative PMT pixel at that location in its FOV. At any time, typically a few percent of the PMTs in the telescopes' cameras are malfunctioning, or are temporarily disabled to avoid damage due to bright stars.

4. Analysis Verification using the CALIOP Instrument on the CALIPSO Satellite

The probability of the VERITAS array triggering on and recording an optical pulse, as well as the efficiency of the subsequent analysis, is difficult to test under realistic conditions. Monte Carlo simulations provide one approach and are commonly used to estimate the effective detection area and to define the analysis and event selection cuts for gamma-ray astronomy. In this case, the simulated gamma-ray events can be compared with a known bright source of astrophysical gamma-rays, such as the Crab Nebula, and the telescope model parameters tuned until a satisfactory match is achieved. For the analysis, however, no natural standard signal exists with which to compare simulations, or to verify the analysis. Furthermore, the precise properties of the pulse to be simulated (rise time, pulse width, wavelength, etc.) are not known.

An ideal test signal would be a distant laser that flashes the telescope cameras from a known location, as this matches the technosignature we are looking for. Pulsed light sources have been used for the calibration of IACTs for many years. From 2005, nightly calibrations of VERITAS were performed using a laser with a 337 nm wavelength and a pulse duration of 4 ns at a distance of roughly 5 m from the camera (Hanna 2008) before switching to a similar LED-based calibration system in 2010 (Hanna et al. 2010). However, these measurements are designed to illuminate the entire FOV uniformly and do not serve as a useful analog to a distant point source. Another calibration technique once used by VERITAS involves firing a laser pulse upwards from the ground and observing the Rayleigh-scattered laser light with the telescopes (Shepherd et al. 2005; Hanna 2008). Again, the observed image is not point-like, but corresponds to an illuminated column in the atmosphere.

The Cloud-Aerosol Lidar with Orthogonal Polarization (CALIOP) instrument on board the polar orbiter Cloud-Aerosol Lidar and Infrared Pathfinder Satellite Observation (CALIPSO) satellite is a space-based backscattering lidar, designed to provide high-resolution vertical profiles of aerosols and clouds, which emits 110 mJ, 20 ns duration laser pulses at a repetition rate of 20.16 Hz, at both 532 nm and 1064 nm (Winker et al. 2009). This provides an excellent technosignature verification source for VERITAS. The camera PMTs are sensitive at 532 nm, with a quantum efficiency of approximately 12%. At an orbital height of 700 km, the laser is effectively a point source at infinity relative to the size of VERITAS. The lidar is directed 3° from the geodetic nadir in the forward along-track direction of the satellite's orbit, and the laser footprint on the ground is predicted to be less than 100 m in diameter (Winker et al. 2009), making a coincidental overlap with the VERITAS telescopes extremely unlikely. However, observations by the TAIGA-HiScore collaboration of the CALIPSO laser (Porelli & Taiga Collaboration 2022) demonstrated that the actual footprint extends far beyond the nominal distance, out to at least tens of kilometers, for reasons which are not entirely clear. This motivated both new observations with VERITAS,and a search of the VERITAS archive for serendipitous passages of the satellite through the field of view.

Examples of these CALIPSO observations are shown in Figure 3. The top image illustrates a passage from a dedicated observation on 2021 May 17, which occurred at an elevation of 74°. The pulse intensity observed by VERITAS was approximately 2000 photoelectrons at each telescope, corresponding to 150 photons m^{-2} at ground level. During the transit, 69% of the pulses emitted by CALIPSO triggered VERITAS and 55% passed the optical SETI analysis cuts without accounting for the *loss* parameter. The efficiency without the *loss* cut applied is most relevant for comparison with our analysis, as we select target locations that are not close to the camera edge (Section 5). For these very-high-intensity pulses, the missing triggered events are largely explained by the dead time of the telescope data acquisition (which was 9% for this observation) and by the existence of a large patch of inoperative PMTs in one telescope along the track of the satellite, as can be seen in the figure.

A second transit is shown at the bottom of Figure 3. This was a serendipitous passage, which occurred on 2013 November 11 at an elevation of 54°, when the center of the laser footprint was ∼400 km distant from the location of VERITAS. The measured pulse intensity is more than an order of magnitude lower in this case, corresponding to approximately 10 photons m^{-2}. 21% of the pulses emitted by CALIPSO triggered VERITAS and 20% passed our analysis without accounting for *loss*. The relatively

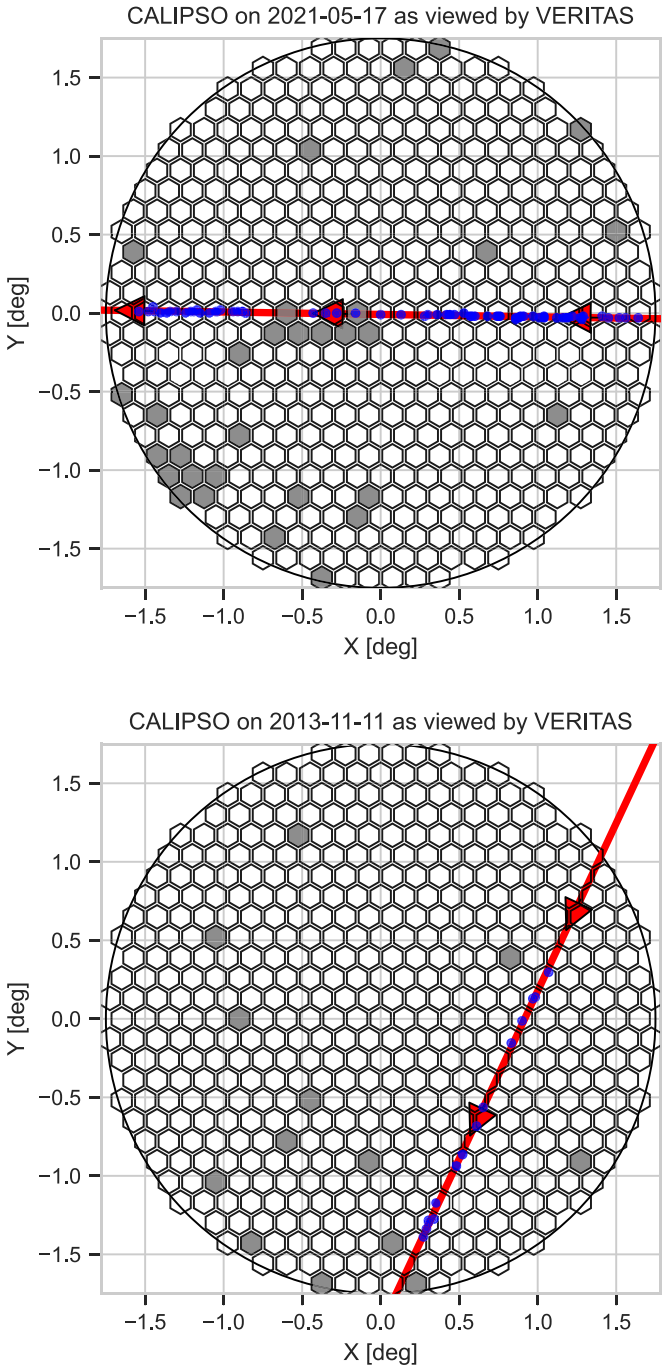

Figure 3. Tracks of the CALIPSO transits (in camera coordinates) on 2021 May 17 (top) and 2013 November 11 (bottom) with the location of the average of the image centers in an event shown as blue points. The hexagons correspond to VERITAS pixels. Grayed-out pixels were nonfunctional during the transit for VERITAS telescope 1.

low trigger efficiency during this transit is likely the result of the extremely nonuniform sensitivity of the VERITAS trigger system to point-like pulses, as we discuss in more detail in Section 6.

5. Observations and Results

The VERITAS/Breakthrough Listen search we have conducted comprises two datasets, which we describe below. The first of these is a program of dedicated VERITAS observations of Breakthrough Listen targets, while the second is an analysis of serendipitous archival observations.

5.1. Dedicated VERITAS Observations

Between 2019 March and 2020 March, VERITAS spent 30 hr observing objects selected from the Breakthrough Listen target catalog (Isaacson et al. 2017). This catalog lists targets originally identified for Breakthrough Listen observations with the Green Bank Telescope, Parkes Telescope, and the Automated Planet Finder. It includes: the 60 nearest stars; 1649 stars within a distance of 50 pc sampling a range of masses, ages, and elemental abundances; 123 nearby galaxies; and several exotic objects, including white dwarfs, brown dwarfs, neutron stars, and black holes.

Not all of these targets are suitable for observations with VERITAS. We removed all galaxies, on the assumption that optical emission is unlikely to be detectable over such large (i.e., extragalactic) distances (Hippke 2018). We also limited targets to the decl. band between $\delta = -10^{\circ}$ and $\delta = +70^{\circ}$, to ensure that the object culminates above $\sim 40^{\circ}$. High-elevation observations are preferred, as they provide greater discrimination power between a pulsed point source at infinity and the background of Cherenkov events generated in the Earth's atmosphere. This is due to the fact that Cherenkov flashes observed at low elevation occur at a larger distance from the telescopes, reducing their parallax angle, image intensity, and angular size and making them appear more point-like.

We also removed all targets with a B-band magnitude of less than 7, and all targets within $0\overset{\circ}{.}15$ of an object (excluding the target itself) with a B or V magnitude of less than 8. Bright stars generate a large amount of background photon noise in the VERITAS PMTs, as well as high currents, which accelerate wear. If the current on any individual PMT exceeds a preset threshold, the high voltage supplied to that channel is automatically turned off. This has little impact on the observation of Cherenkov events with large angular extent, but reduces or completely removes the sensitivity to point-like optical pulses from the star's location.

Finally, we removed any targets which had been previously observed by VERITAS, either intentionally or serendipitously, in the FOV of other observations. Observations of these targets are included in the archival search described in Section 5.2. This resulted in a list of 506 targets, which were then ranked according to the inverse square of their distance and their optical brightness, with nearby, optically faint targets being preferred. Targets lying close to the ecliptic (which could host civilizations that view the Earth as a transiting exoplanet Heller & Pudritz 2016; Sheikh et al. 2020), or hosting known exoplanets, or located close to another target, were also favored, but with lower weight than the two main criteria of brightness and distance.

Candidates from this target list were selected for observation based on their ranking and on observatory scheduling constraints. Observations were conducted in typically 15 minute exposures taken within 90 minutes of culmination, with the primary target offset from the center of the FOV by $1\overset{\circ}{.}25$. This offset was chosen to improve the probability of triggering a faint pulse, as discussed in more detail in Section 6.1. All data were taken under clear skies, at new or crescent Moon phases, and with all four telescopes in the array operating correctly. The final data set comprises 127 observing runs of 108 nonoverlapping target fields, with a total exposure

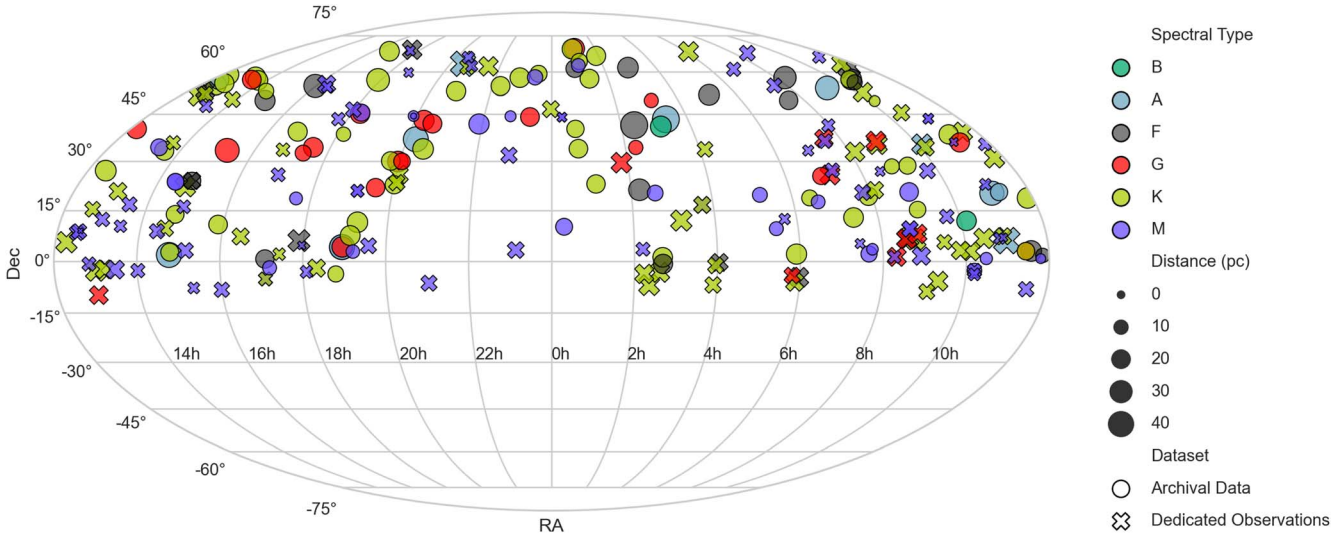

Figure 4. Stellar target locations, in equatorial coordinates, for both the dedicated and archival VERITAS observations. Distance and spectral type are also indicated, as described in the figure legend.

of 30.16 hr. Some target fields contain multiple targets, allowing us to study a total of 136 targets with this data set. Most targets were observed only once, while 25 were observed twice, and three were observed three times.

The locations of the observed stellar targets are shown in Figure 4, with their spectral class and distance indicated. Figure 5 shows the Hertzsprung–Russell diagram for all of the stellar Breakthrough Listen targets, with those targets observed by VERITAS indicated. The VERITAS selection covers a broad range of spectral classes along the main sequence, from B to M, as well as a few giant branch stars.

5.2. Archival Search

VERITAS has been fully operational since 2007, and records typically ∼1000 hr of observations each year. Thanks to the large VERITAS FOV (9.6 deg^2), these observations provide coverage of over 20% of the sky, with exposures cumulatively ranging from a few minutes to hundreds of hours. A complete search of this extensive archive for optical pulses is a worthwhile subject for future work but will require further development of the analysis tools—in particular, to deal with observations recorded at low elevation and to overcome the increased background from examining the entire FOV as opposed to just the region around a set of predefined locations.

For this work, we selected a reduced set of archival VERITAS observations to analyze. To create this set, we required that the observations were recorded at high elevations (>40°), with at least three telescopes operating, and with excellent weather conditions. Data taken prior to the summer of 2012 were not considered, as this was when the VERITAS photomultiplier tube cameras were upgraded, improving the photon detection efficiency by ∼30% (Kieda 2013). Unlike the dedicated observations, the radial distance of the target from the center of the field of view for archival observations could not be fixed at 1°.25. We instead set the maximum radial distance to be 1°.5. We also set the maximum exposure to be analyzed on any single target to be 1 hr. If any target exceeded this threshold, we analyzed the first hour of good-quality data and left the remainder for future full archival analysis. With these conditions, we selected 249 archival observations with an

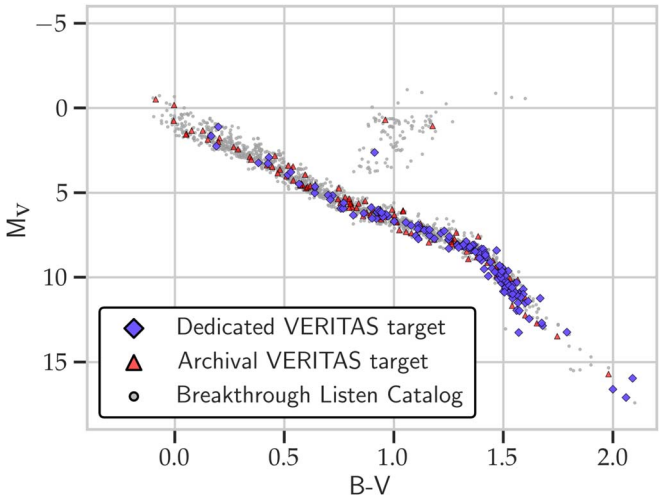

Figure 5. Coverage across an H-R diagram for the stellar targets used in both dedicated observations and archival analysis. It is similar to the coverage found in the original Isaacson et al. (2017) catalog.

average length of 28 minutes which altogether represents 110 hr of observations containing 140 individual Breakthrough Listen targets and 119 nonoverlapping fields. The list of Breakthrough Listen targets in this archival data set includes 25 galaxies, which were serendipitously inside the studied fields and are included here for completeness. This data set constitutes all of the Breakthrough Listen targets for which we have good-quality, high-elevation data taken between 2012 September and 2019 March. We note that the entire VERITAS archive comprises almost 20,000 hr of data, including additional observations of the Breakthrough targets analyzed here. The full analysis of this data set will be presented in future work. Figure 4 shows the location, spectral type, distance, and originating data set of all analyzed targets. Figure 5 shows the same targets, but instead within the H-R diagram, showing the color and magnitude of the targets. As the figures show, the analyzed targets selected occupy a significant portion of the parameter space—locations, distances, and spectral properties—of the Isaacson et al. (2017) catalog.

Table 1
Number of Events Remaining after Each Stage of the Analysis

Cut Description	Events Remaining after Cut	
	Archival Data	Dedicated Observations
Before cuts	127,346,295	34,917,340
At least three images	80,910,174	23,088,334
Point-like images (third-smallest length $< 0.^{\circ}09$ and width $< 0.^{\circ}07$)	1,894,155	508,637
Image centers co-located (within $0.^{\circ}15$)	237	35
Near target (within $0.^{\circ}15$)	3	1
Images are not truncated (loss = 0)	3	1
Visual inspection	0	0
Candidate Events	0	0

5.3. Results

Table 1 shows the results of each stage of the analysis pipeline for both the dedicated observations and for the archival data set. For the dedicated observations, only one event survived the predefined selection cuts (target HIP 83043). For the larger archival data set, three events survived (targets HIP 51317, HIP 93871, and NGC 4551) and were subjected to visual inspection. For three of these four events, two of the four telescopes in the array triggered and three of the four telescopes registered an image. The fourth telescope did not, despite being operational and having no disabled PMTs at the pulse location. These events therefore fail our requirement for uniform intensity and are rejected. The remaining event shows three OSETI-like images, thereby satisfying the third-smallest *width* and *length* criterion, but the fourth telescope image contains a bright, extended flash, with an angular (parallactic) displacement from the other images. This clearly identifies the event as being due to a cosmic-ray air shower in the atmosphere, and so it is also rejected. We therefore have zero candidate events remaining after the full analysis.

6. Discussion

We have presented the analysis of observations of 272 Breakthrough Listen targets with VERITAS (there are four targets in common between the target lists of the dedicated observations and the archival search) and have found no evidence for rapid optical pulses from any of these objects. Here we attempt to summarize the sensitivity of our search, both in terms of the minimum optical pulse intensity detectable by VERITAS and in the constraints our survey allows us to place on the frequency of emitting civilizations.

6.1. Optical Pulse Sensitivity

Abeysekara et al. (2016) estimated the minimum optical pulse intensity detectable by VERITAS to be 0.94 photons m^{-2} for a 12 ns integration window while noting that such estimates are challenging due to the various unknown pulse properties (location, wavelength, duration, temporal profile, etc). The CALIPSO observations demonstrate experimentally that pulses with an intensity of 10 photons m^{-2} can be detected. Furthermore, the CALIPSO pulses are relatively long duration, with a pulse width of ∼20 ns. The single photoelectron pulse width for VERITAS is 4 ns, and the camera trigger coincidence time is ∼5 ns, implying that shorter pulses with a substantially lower integrated photon intensity must also be detectable. However, the CALIPSO results also highlight that the efficiency of pulse detection with VERITAS is not 100%. We discuss one of the reasons for this in more detail here.

As mentioned, the VERITAS telescope cameras are each composed of 499 photomultiplier tubes on a hexagonal grid, with a pixel-to-pixel spacing of $0.^{\circ}15$. For an individual telescope to trigger on an optical pulse, signals on three adjacent PMT pixels must exceed a discriminator threshold within a ∼5 ns coincidence window. A laser pulse generated at a large distance is point-like, and so this three-adjacent trigger condition would never be met, if the optical system were perfect. In reality, an image of a point source has the same shape and structure as the telescope optical PSF, which may overlap multiple pixels. The angular extent of Cherenkov showers and the PMT pixels allows for cheaper mirrors with a significantly reduced angular resolution/increased PSF compared to typical optical telescopes. This means that IACTs like VERITAS can be much larger and overall cheaper than their optical counterparts (Canestrari et al. 2010). The PSF will also vary across the field of view due to comatic aberration. At the center of the camera, it can be approximated by a bivariate Gaussian with a $\sim 0.^{\circ}08$ 68% containment diameter, increasing to $\sim 0.^{\circ}15$ at an offset of $1.^{\circ}2$, and degrading further toward the edge of the camera at $1.^{\circ}75$.

The probability of satisfying the three-adjacent trigger condition therefore depends very strongly upon the exact pulse location in the field of view. In particular, it is determined by the amount of light received by the PMT which is third-most-distant from the image centroid—i.e., that which measures the third-largest signal. In the most favorable case, the pulse centroid location lies equidistant between three pixels, each of which receives approximately one-third of the light. In the least favorable case, the pulse lands exactly in the center of a pixel, and adjacent pixels receive only a small fraction of the light. The difference between these two cases is the most extreme close to the camera center, where the optical PSF is small, and the least extreme at the camera edge, where the optical PSF is more extended.

Figure 6 shows the results of a Monte Carlo simulation which illustrates these effects and how the minimum pulse sensitivity varies with radial distance in the camera. The optimum sensitivity is taken to be the same as that estimated by Abeysekara et al. (2016). The green dotted line in the figure corresponds to the worst case, where the pulse is centered on a pixel. The blue solid line corresponds to the best case, where the pulse is equidistant between 3 pixels. For a random pulse location on the camera, the most likely distance between the pulse location and the pixel containing the third brightest signal is $0.^{\circ}13$. The orange dashed line indicates this typical case. 75% of possible pulse locations in the camera provide a sensitivity equal to or better than this typical case. The cross-hatched region indicates this, as well as the outer region of the camera corresponding to 75% of the total area. The black vertical line at a camera radius of $1.^{\circ}25$ indicates the position of the Breakthrough Listen targets in the field of view for the dedicated VERITAS observations reported here. The typical sensitivity in this case is 3 ph m^{-2}. Observations of the CALIPSO satellite laser over a wide range of elevations (and hence pulse intensity and pulse location in the cameras) are currently being taken by VERITAS and will allow testing these sensitivity estimates more rigorously.

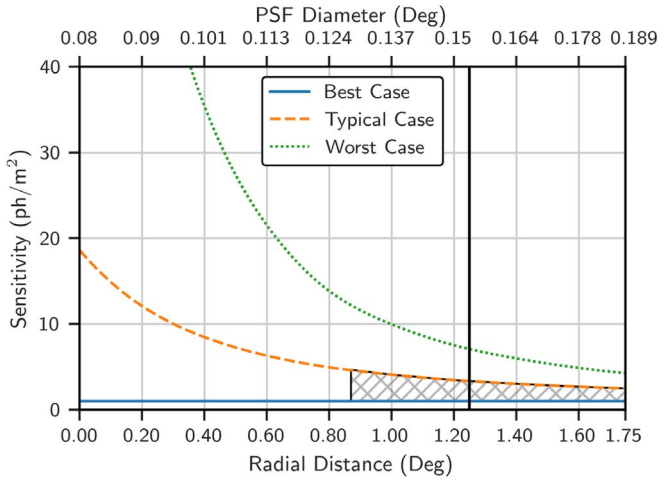

Figure 6. Sensitivity (minimum detectable pulse intensity) as a function of the radial distance from the center of the VERITAS telescope field of view. The three curves correspond to a pulse located at the center of a PMT (worst case), equidistant between three PMTs (best case), and at the most common location (typical case). The crosshatched region indicates the outer 75% of the camera area and the sensitivity of 75% of the possible pulse locations within this area. See the text for more details.

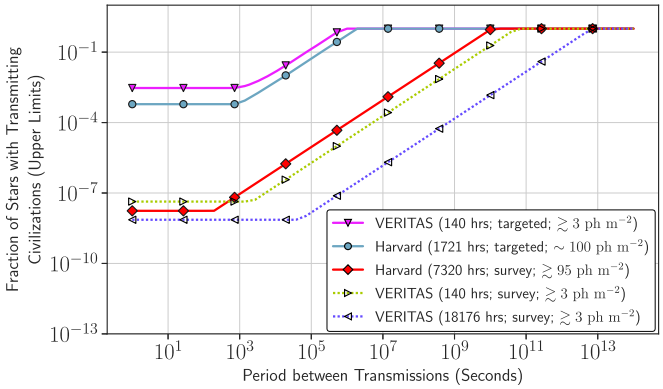

Figure 7. Upper limits on the fraction of stars with transmitting civilizations as a function of the average period between pulses, using the model from Howard et al. (2007; building on Howard et al. 2004) which assumes no candidate pulses are found. From top to bottom the five lines correspond to: all data from this paper (247 targets; upside-down triangles), the Harvard targeted search (Howard et al. 2004; 4730 targets, circles), the Harvard All-Sky nontargeted survey (Howard 2006; Mead 2013; 7320 hr, diamonds), a hypothetical nontargeted VERITAS survey using all of the data from this paper (140 hr; right-pointing triangles), and a hypothetical nontargeted survey using all data from the entire VERITAS archive (18,176 hr; left-pointing triangles). The minimum detectable pulse is ∼30 times larger for Harvard than for VERITAS.

As a final point, we stress that the issue of nonuniform sensitivity across the field of view is not intrinsic to the technique; rather, it is a result of the VERITAS trigger system design, which is optimized for gamma-ray astronomy. A dedicated trigger for point-like optical pulses, requiring the same single pixel to cross a trigger threshold on multiple separated telescopes, would completely remove this limitation. This could be implemented in a relatively straightforward manner on existing or future facilities and operate in parallel with the existing Cherenkov trigger system.

6.2. Survey Sensitivity

The sensitivity to optical pulses is an important instrumental metric. Complementary to this, however, is the sensitivity of the search as a survey: that is, how do our results constrain the parameter space of potential emitters? There are many different ways to estimate this, usually discussed in the context of searches for radio technosignatures (e.g., see Wright et al. 2018a and references therein). The most applicable prior works for our purposes are those of Howard et al. (2004, 2007), and Mead (2013) which discuss the search for nanosecond-duration, pulsed optical emission using optical astronomical telescopes equipped with hybrid avalanche photodetectors or with photomultiplier tubes. From 1998 to 2003, 11,600 targeted observations of 4730 stellar objects were made under good conditions with the 1.5 m aperture Wyeth telescope at the Harvard/Smithsonian Oak Ridge Observatory, with a total exposure of 1721 hr. Subsequently, the Harvard All-Sky Observatory utilized a custom optical setup consisting of a 1.8 m telescope that focused a $1.^{\circ}6 \times 0.^{\circ}2$ patch of the sky onto a beam splitter with matched arrays of eight photomultiplier tubes down each path. From 2007 to 2012, it made 7320 hr of observations over which it searched the entire northern sky four times.

Each of these campaigns used the same mathematical model, as explained in Howard et al. (2004), to place an upper bound on the fraction of nearby stars that host civilizations emitting optical pulses toward the Earth as a function of P, the typical pulse repetition period, under the assumption that any emitted pulse would exceed the minimum pulse sensitivity of the instrument. The results are replicated in Figure 7. We emphasize, however, that the minimum pulse sensitivity of the VERITAS observations ($\gtrsim$3 ph m^{-2}) is much better than that of the Harvard experiment ($\gtrsim$100 ph m^{-2}).

We have applied a similar methodology to the sum of both VERITAS data sets described in this paper, with an observed sample of 247 unique stellar targets, and a total observation time of 140 hr. Figure 7 also demonstrates the potential survey sensitivity that can be achieved if we still obtain no candidate events after removing the constraint that pulses must be associated with a predefined location from the Breakthrough Listen target list. This requires some additional analysis development, to further reduce the remaining background, but is realistically achievable in the near future. For this calculation, we assume a typical stellar density of 0.1 stars pc^{-3} and a maximum range of 1 kpc, corresponding to 4×10^8 stars over the whole sky—similar to the values used for calculating the Harvard All-Sky limits (Mead 2013). Using only the 140 hr data set considered in this paper, this search would lower the upper limit on the fraction of stars with transmitters by roughly five orders of magnitude, corresponding to the ratio of the number of stars searched between targeted and nontargeted techniques. Applying the same approach to the entire VERITAS archive of 18,176 hr would further reduce the minimum upper limit, and extend the search sensitivity to much longer pulse transmission periods.

7. Conclusions and Prospects

VERITAS is not alone in searching for optical technosignatures. Table 1 in Schuetz et al. (2016) summarized the capabilities of optical technosignature searches at the time of the VERITAS analysis of KIC 462852. Since then, there have been numerous developments in the field. The Near-InfraRed Optical SETI instrumentation on a 1 m telescope at the Lick Observatory has been used to conduct a survey of 1280 celestial objects in the near-infrared (950–1650 nm), sensitive

to pulses with durations of <50 ns (Maire et al. 2019). Tellis & Marcy (2017) conducted a survey of 5600 FGKM stars using the Keck 10 m telescope, searching for a spectral (not temporal) signature of laser emission. An all-sky instrument called PANOSETI is under development (Liu et al. 2020; Maire et al. 2022), and will soon provide nightly all-sky coverage from two sites. Cherenkov telescopes also have an important role to play in future developments. The TAIGA-HiSCORE wide-aperture Cherenkov array, consisting of 100, 0.5 m^2 telescopes spread over 1 km^2 with a field of view of 0.6 sr, has searched for nanosecond optical transients and detected pulsed emission from the CALIPSO satellite (Adams et al. 2022). In the coming decade, the Cherenkov Telescope Array (CTA) will provide unprecedented telescope light collecting area, exceeding the mirror area of all of the world's large optical telescopes combined (Cherenkov Telescope Array Consortium et al. 2019). It will have the capability to conduct nanosecond optical pulse searches similar to VERITAS, with much greater sensitivity and stricter background rejection. As we have shown here, verification and calibration of this capability with satellite-based lasers will be an important component of this program, as will considerations of the optical performance and trigger system design of the telescope.

Acknowledgments

This research is supported by grants from the U.S. Department of Energy Office of Science, the U.S. National Science Foundation, and the Smithsonian Institution, by NSERC in Canada, and by the Helmholtz Association in Germany. This research used resources provided by the Open Science Grid, which is supported by the National Science Foundation and the U.S. Department of Energy's Office of Science, and resources of the National Energy Research Scientific Computing Center (NERSC), a U.S. Department of Energy Office of Science User Facility operated under Contract No. DE-AC02-05CH11231. We thank the Breakthrough Prize Foundation and the University of California, Berkeley, for their support. We also acknowledge the excellent work of the technical support staff at the Fred Lawrence Whipple Observatory and at the collaborating institutions in the construction and operation of the instrument.

Services: Celestrak, NASA Exoplanet Archive, TeVCat, SIMBAD database, ViZieR catalog access tool.

Software: ROOT (Antcheva et al. 2009), Astropy (Astropy Collaboration et al. 2022), Astroquery (Ginsburg et al. 2019), BeautifulSoup, GeoPy, Matplotlib (Hunter 2007), Mechanize, NetworkX (Hagberg et al. 2008), Numpy (Harris et al. 2020), Pandas (McKinney 2010), PyTeVCat, Seaborn (Waskom 2021), Skyfield (Rhodes 2020).

ORCID iDs

A. Acharyya https://orcid.org/0000-0002-2028-9230
C. B. Adams https://orcid.org/0000-0002-9021-6192
P. Bangale https://orcid.org/0000-0002-3886-3739
P. Batista https://orcid.org/0000-0001-8138-1391
W. Benbow https://orcid.org/0000-0003-2098-170X
A. Brill https://orcid.org/0000-0002-6208-5244
M. Capasso https://orcid.org/0000-0002-8136-9461
M. Errando https://orcid.org/0000-0002-1853-863X
A. Falcone https://orcid.org/0000-0002-5068-7344
Q. Feng https://orcid.org/0000-0001-6674-4238
G. M. Foote https://orcid.org/0000-0002-2944-6060
L. Fortson https://orcid.org/0000-0002-1067-8558
A. Furniss https://orcid.org/0000-0003-1614-1273
W. Hanlon https://orcid.org/0000-0002-0109-4737
D. Hanna https://orcid.org/0000-0002-8513-5603
O. Hervet https://orcid.org/0000-0003-3878-1677
C. E. Hinrichs https://orcid.org/0000-0001-6951-2299
J. Holder https://orcid.org/0000-0002-6833-0474
T. B. Humensky https://orcid.org/0000-0002-1432-7771
W. Jin https://orcid.org/0000-0002-1089-1754
P. Kaaret https://orcid.org/0000-0002-3638-0637
D. Kieda https://orcid.org/0000-0003-4785-0101
T. K. Kleiner https://orcid.org/0000-0002-4260-9186
N. Korzoun https://orcid.org/0000-0002-4289-7106
S. Kumar https://orcid.org/0000-0002-5167-1221
M. J. Lang https://orcid.org/0000-0003-4641-4201
M. Lundy https://orcid.org/0000-0003-3802-1619
G. Maier https://orcid.org/0000-0001-9868-4700
M. J. Millard https://orcid.org/0000-0001-7106-8502
C. L. Mooney https://orcid.org/0000-0001-5937-446X
P. Moriarty https://orcid.org/0000-0002-1499-2667
R. Mukherjee https://orcid.org/0000-0002-3223-0754
S. O'Brien https://orcid.org/0000-0002-9296-2981
R. A. Ong https://orcid.org/0000-0002-4837-5253
M. Pohl https://orcid.org/0000-0001-7861-1707
E. Pueschel https://orcid.org/0000-0002-0529-1973
J. Quinn https://orcid.org/0000-0002-4855-2694
K. Ragan https://orcid.org/0000-0002-5351-3323
D. Ribeiro https://orcid.org/0000-0002-7523-7366
J. L. Ryan https://orcid.org/0000-0001-6662-5925
I. Sadeh https://orcid.org/0000-0003-1387-8915
L. Saha https://orcid.org/0000-0002-3171-5039
M. Santander https://orcid.org/0000-0001-7297-8217
R. Shang https://orcid.org/0000-0002-9856-989X
D. A. Williams https://orcid.org/0000-0003-2740-9714
S. L. Wong https://orcid.org/0000-0002-2730-2733
J. Woo https://orcid.org/0009-0001-6471-1405
D. DeBoer https://orcid.org/0000-0003-3197-2294
H. Isaacson https://orcid.org/0000-0002-0531-1073
I. de Pater https://orcid.org/0000-0002-4278-3168
D. C. Price https://orcid.org/0000-0003-2783-1608
A. Siemion https://orcid.org/0000-0003-2828-7720

References

Abeysekara, A. U., Archambault, S., Archer, A., et al. 2016, ApJL, 818, L33
Adams, C. B., Benbow, W., Brill, A., et al. 2022, A&A, 658, A83
Antcheva, I., Ballintijn, M., Bellenot, B., et al. 2009, CoPhC, 180, 2499
Armada, A., Cortina, J., & Martinez, M. 2005, in Neutrinos and Explosive Events in the Universe, ed. M. M. Shapiro, T. Stanev, & J. P. Wefel (Dordrecht: Springer), 307
Astropy Collaboration, Price-Whelan, A. M., Lim, P. L., et al. 2022, ApJ, 935, 167
Bracewell, R. N. 1960, Natur, 186, 670
Canestrari, R., Motta, G., Pareschi, G., et al. 2010, Proc. SPIE, 7739, 77390H
Cherenkov Telescope Array Consortium, Acharya, B. S., Agudo, I., et al. 2019, in Science with the Cherenkov Telescope Array, ed. CTA Consortium (Singapore: World Scientific)
Cocconi, G., & Morrison, P. 1959, Natur, 184, 844
Cogan, P. 2008, ICRC (Yucatán), 3, 1385
Covault, C. E. 2001, Proc. SPIE, 4273, 161
Davies, J. M., & Cotton, E. S. 1957, SoEn, 1, 16
Dyson, F. J. 1960, Sci, 131, 1667
Eichler, D., & Beskin, G. 2001, AsBio, 1, 489
Franz, N., Croft, S., Siemion, A. P. V., et al. 2022, AJ, 163, 104
Gajjar, V., Siemion, A., Croft, S., et al. 2019, BAAS, 51, 223
Gingrich, D. M., Boone, L. M., Bramel, D., et al. 2005, ITNS, 52, 2977

Ginsburg, A., Sipőcz, B. M., Brasseur, C. E., et al. 2019, AJ, 157, 98
Hagberg, A. A., Schult, D. A., & Swart, P. J. 2008, in Proc. of the 7th Python in Science Conf., ed. G. Varoquaux, T. Vaught, & J. Millman (Pasadena: ScyPy), 11
Hanna, D. 2008, ICRC (Yucatán), 3, 1417
Hanna, D., McCann, A., McCutcheon, M., & Nikkinen, L. 2010, NIMPA, 612, 278
Hanna, D. S., et al. 2009, AsBio, 9, 345
Harris, C. R., Millman, K. J., van der Walt, S. J., et al. 2020, Natur, 585, 357
Heller, R., & Pudritz, R. E. 2016, AsBio, 16, 259
Hillas, A. M. 1985, 19th ICRC (San Diego), 3, 445
Hippke, M. 2018, JApA, 39, 73
Holder, J. 2021, in Gamma-Ray and Multimessenger Astronomical Instrumentation, ed. D. N. Burrows, 5 (2nd ed.; Singapore: World Scientific), 117
Holder, J., Ashworth, P., LeBohec, S., Rose, H. J., & Weekes, T. C. 2005, 29th ICRC (Pune), 5, 387
Holder, J., Atkins, R. W., Badran, H. M., et al. 2006, APh, 25, 391
Horowitz, P., Coldwell, C. M., Howard, A. B., et al. 2001, Proc. SPIE, 4273, 119
Howard, A., Horowitz, P., Mead, C., et al. 2007, AcAau, 61, 78
Howard, A. W. 2006, PhD thesis, Harvard Univ.
Howard, A. W., Horowitz, P., Wilkinson, D. T., et al. 2004, ApJ, 613, 1270
Hunter, J. D. 2007, CSE, 9, 90
Isaacson, H., Siemion, A. P. V., Marcy, G. W., et al. 2019, PASP, 131, 014201
Isaacson, H., Siemion, A. P. V., Marcy, G. W., et al. 2017, PASP, 129, 054501
Kieda, D. B. 2013, ICRC (Rio de Janeiro), 33, 1124
Krause, M., Pueschel, E., & Maier, G. 2017, APh, 89, 1
Lipman, D., Isaacson, H., Siemion, A. P. V., et al. 2019, PASP, 131, 034202
Liu, W., Werthimer, D., Lee, R., et al. 2020, Proc. SPIE, 11447, 114477G
Maier, G., & Holder, J. 2017, ICRC (Busan), 301, 747
Maire, J., Wright, S. A., Barrett, C. T., et al. 2019, AJ, 158, 203
Maire, J., Wright, S. A., Holder, J., et al. 2022, Proc. SPIE, 12184, 121848B
McCann, A., Hanna, D., Kildea, J., & McCutcheon, M. 2010, APh, 32, 325
McKinney, W. 2010, in Proc. of the 9th Python in Science Conf., ed. S. van der Walt & J. Millman (Austin: SciPy), 56
Mead, C. C. 2013, PhD thesis, Harvard Univ.
Nagai, T., McKay, R., Sleege, G., & Petry, D. 2008, ICRC (Yucatán), 3, 1437
Porelli, A. & Taiga Collaboration 2022, ICRC (Berlin), 37, 876
RhodesB. (2020) Skyfield: Generate high precision research-grade positions for stars, planets, moons, and earth satellites1, v. 1.45 Astrophysics Source Code Library, ascl:1907.024
Roache, E., Irvin, R., Perkins, J. S., et al. 2008, ICRC (Yucatán), 3, 1397
Schneider, J., Léger, A., Fridlund, M., et al. 2010, AsBio, 10, 121
Schuetz, M., Vakoch, D. A., Shostak, S., & Richards, J. 2016, ApJL, 825, L5
Schwartz, R. N., & Townes, C. H. 1961, Natur, 190, 205
Sheikh, S. Z., Siemion, A., Enriquez, J. E., et al. 2020, AJ, 160, 29
Shepherd, N., Buckley, J. H., Celik, O., et al. 2005, ICRC (Pune), 5, 427
Siemion, A., Benford, J., Cheng-Jin, J., et al. 2015, in Advancing Astrophysics with the Square Kilometre Array, 14, (Proc. of Science), 116
Tarter, J. 2003, in Proceedings of the Conference on Towards Other Earths: DARWIN/TPF and the Search for Extrasolar Terrestrial Planets, ed. M. Fridlund, T. Henning, & H. Lacoste (Noordwijk: ESA Publications Division), 31
Sullivan, W. T. I., Brown, S., & Wetherill, C. 1978, Sci, 199, 377
Tellis, N. K., & Marcy, G. W. 2017, AJ, 153, 251
Traas, R., Croft, S., Gajjar, V., et al. 2021, AJ, 161, 286
Turnbull, M. C., & Tarter, J. C. 2003, ApJS, 145, 181
Waskom, M. L. 2021, JOSS, 6, 3021
Winker, D. M., Vaughan, M. A., Omar, A., et al. 2009, J. Atmos. Sci. Oceanic Sci., 26, 2310
Worden, S. P., Drew, J., Siemion, A., et al. 2017, AcAau, 139, 98
Wright, J. T. 2018, in Handbook of Exoplanets, ed. H. J. Deeg & J. A. Belmonte (Cham: Springer), 3405
Wright, J. T., Kanodia, S., & Lubar, E. 2018a, AJ, 156, 260
Wright, J. T., Sheikh, S., Almár, I., et al. 2018b, arXiv:1809.06857
Wright, S. A., Horowitz, P., Maire, J., et al. 2018c, Proc. SPIE, 10702, 107025I
Zuckerman, A., Ko, Z., Isaacson, H., et al. 2023, AJ, 165, 114